Cross Polarization for ^{1}H NMR Image Contrast in Solids

Toshihito Nakai, Yasuhiro Fukunaga, Masayuki Nonaka, Shigeru Matsui,[1] and Tamon Inouye

Institute of Applied Physics, University of Tsukuba, Tsukuba, Ibaraki 305-8573, Japan

E-mail: matsui@bk.tsukuba.ac.jp

A novel ^{1}H imaging method for solids, yielding images reflecting ^{1}H–^{13}C dipolar interactions through cross relaxation time T_{IS}, is presented. Phase-alternating multiple-contact cross polarization (PAMC CP) was incorporated into the magic-echo frequency-encoding imaging scheme; the PAMC CP sequence may partly but efficiently destroy the initial ^{1}H magnetization depending on the T_{IS} values. A theory describing the effects of the PAMC CP sequence was developed, which was used for the assessment of the sequence as well as the analysis for the experimental results. It was demonstrated that the T_{IS}-weighted ^{1}H image and the T_{IS} mapping for a phantom, constituted of adamantane and ferrocene, can distinguish these compounds clearly.   © 1998 Academic Press

Key Words: cross polarization; cross relaxation time T_{IS}; solid-state imaging; image contrast; ^{1}H–^{13}C dipolar interaction.

INTRODUCTION

In contrast to the flourish of its medical application, NMR imaging for solid materials is still at the stage of developing (*1*). The cause hampering easy access to the solid-state imaging may eventually be the variety and magnitude of the interactions to which nuclear spins in solids are liable; the broadenings of resonance lines due to dipolar interactions, for instance, may restrict the achievable resolution of the resultant NMR images. Much attention is paid and many efforts are made to overcome the broadenings for the purpose of high-resolution solid-state NMR imaging (*1*). In particular, magic-echo approaches (*2–4*) are probably one of the most promising, and their application to nondestructive analysis of solid materials has been producing a fruitful outcome (*1*).

It is worth pointing out that such various spin interactions in solids, on the other hand, may permit a wealth of image contrast to be obtained: The introduction of a variety of contrast is an important subject in general NMR imaging methodology (*5, 6*), enhancing the utility considerably. Although the image contrast may be provided with relaxation phenomena due to spin interactions, by analogy with liquid–state T_1- and T_2-weighting, it is possible for certain contrast to be introduced in a fashion unique to solid-state NMR (*7, 8*). We propose in

the present paper that novel image contrast related with heteronuclear dipolar interactions can be obtained in solid-state NMR imaging. The method particularly exploited here is the one yielding ^{1}H images contrasted by ^{1}H–^{13}C dipolar interactions through cross relaxation time T_{IS} by utilizing cross polarization (CP) (*9–12*). We note that the cross relaxation time T_{IS} could be more sensitive to the degree of cross-linking in elastomers than the other relaxation times like T_2 providing an additional or even more useful image contrast in solid imaging (*13*). A theory necessary for assessing the influences of the CP process on the ^{1}H image contrast is developed, and a T_{IS}-weighted ^{1}H image as well as a T_{IS}-mapping image is experimentally demonstrated.

RESULTS AND DISCUSSION

Experimental Scheme for PAMC CP ^{1}H Imaging

The method we exploit in the present study is the one which can yield ^{1}H images reflecting, as image contrast, the magnitudes of internal ^{13}C–^{1}H dipolar interactions, varying from one compound to another. In order to make the ^{1}H image contrast or the ^{1}H spectral intensity depend on the dipolar interactions, it may occur to us that we can utilize CP (*9–12*) from ^{1}H nuclei to ^{13}C: Some amount of the initial ^{1}H magnetization may be transferred to the ^{13}C nuclei through the CP process promoted by the dipolar interactions, with a time constant T_{IS}, and the surviving ^{1}H magnetization may be offered to the subsequent imaging process. If the amount of the surviving magnetizations is different between materials under study having various values of T_{IS}, the resultant ^{1}H image may acquire the different signal intensities dependent on the materials. It follows that such ^{1}H images may reflect the dipolar interactions as image contrast.

However, it is immediately noticed that the amount of the transferred ^{1}H magnetization via the conventional single-contact CP is not so much as to distinguish the compounds; it is because the heat capacities proportional to the number of the nuclei are so large for the ^{1}H spin system but so small for the ^{13}C system (*10–12*). To make the ^{1}H magnetization decay much more efficiently is, therefore, the central subject in the

---
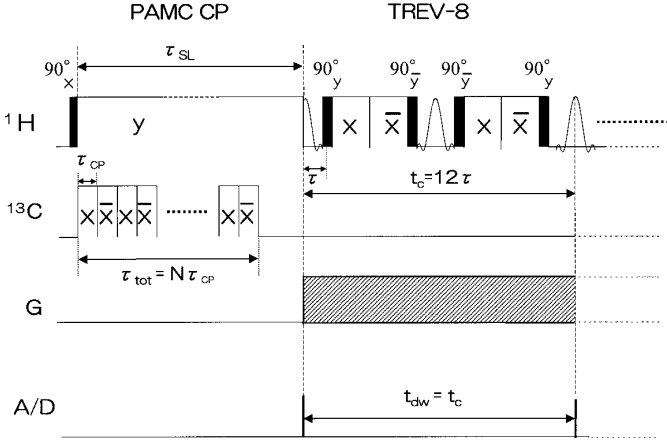
[1] To whom correspondence should be addressed.

FIG. 1. Experimental scheme for PAMC CP (phase-alternating multiple-contact cross polarization) ^{1}H imaging. In the first half of the scheme, ^{1}H transverse magnetization is prepared by PAMC CP RF pulses for ^{1}H and ^{13}C nuclei, whereas in the second half it yields magic echoes during the TREV-8 pulse sequence under the field gradient G. Every other echo is sampled by an A/D converter.

present methodology. For this purpose, we might be able to use the multiple-contact CP (MC CP) which was originally contrived for the indirect detection for the influences of ^{13}C nuclei or for the direct accumulation for the ^{13}C signals (*10–12*). Instead of MC CP, however, we utilize the phase-alternating multiple-contact CP (PAMC CP), which promises more efficient ^{1}H magnetization decay than MC CP, as proved in the next section explicitly.

Figure 1 illustrates the experimental scheme for PAMC CP ^{1}H imaging. In the first half of the sequence is shown PAMC CP for partly destroying the ^{1}H magnetization, and in the second half a TREV-8 subsequence (*15*) with a field gradient for ^{1}H imaging. The PAMC CP subsequence consists of the spin-locking RF field B_{1I} for I(^{1}H) nuclei of the length of τ_{SL} and the phase-alternating fields B_{1S} for S(^{13}C) nuclei. If the Hartmann–Hahn condition, $\gamma_I B_{1I} = \gamma_S B_{1S}$, is satisfied, both the spin systems may contact (*9*). In Fig. 1, each contact time of PAMC CP is represented as τ_{CP}, and the number of the contacts N; as a matter of course, the total contact time is given by $\tau_{tot} = N\tau_{CP}$, which is shorter than or equal to τ_{SL}.

The ^{1}H magnetization partly destroyed by PAMC CP may lead to magic echoes (*14*) in the following TREV-8 subsequence (*15*) as illustrated in Fig. 1. The part of the TREV-8 with a field gradient has already been described by ourselves and others (*2–4*): The ^{1}H signal is sampled at every other echo, since the cycle time of the TREV-8 sequence is $t_c = 12\tau$ where τ is the narrow window of the sequence; namely, the sequence is for the frequency-encoding imaging of the dwelling time $t_{dw} = t_c$. For experimental ease, we use a constant field gradient, instead of the reported fast switching pulse gradients only in the absence of RF irradiation (*2–4*). The effects of the gradient in the burst RF pulses may be of interest, but here they are not discussed and will be reported elsewhere.

Although quantitatively described in the next section, the effect of the PAMC CP sequence on the spin systems is qualitatively outlined as follows: In the first contact, the initial ^{1}H magnetization decays while the ^{13}C magnetization is enhanced. The magnetization transfer from the ^{1}H spin system to the ^{13}C spin system asymptotically stops or slows down, as the spin population of these two systems becomes identical; in other words, the energy transfer stops when the spin temperatures (*10–12*) of both the systems are equalized. In the second contact, however, the population of the ^{13}C spin system is inverted by alternating the phase of the irradiated RF field, or by reversing the quantization axis for the ^{13}C spin system. The magnetization or energy transfer, then, resumes because of the inverted distribution of the ^{13}C spin system differing from that of the ^{1}H system. The above process is repeated N times in the entire PAMC CP sequence, and finally both the ^{1}H and ^{13}C spin systems may completely be *shuffled* and tend to lose their magnetizations. Thus, the ^{1}H magnetization of the present interest may be destroyed efficiently in the PAMC CP sequence.

In practice, the CP process is accompanied by the ^{1}H relaxation process in the rotating frame, or the $T_{1\rho}$ process, during the spin-locking period τ_{SL}. The genuine CP effect is, however, distinguished from the $T_{1\rho}$ effect, by comparing the ^{1}H magnetization surviving after PAMC CP for a fixed length of τ_{SL} and various values of N or τ_{tot}: For a given length of τ_{SL}, the difference of the ^{1}H signals observed with and without N-time multiple contacts is ascribed purely to the CP process. The $T_{1\rho}$ effect during τ_{SL} is thus excluded from our interest throughout the present paper, unless otherwise stated.

[1]H Magnetization Decay During PAMC CP Sequence

The behavior of the I(^{1}H) magnetization decay during the PAMC CP sequence can be formulated by assuming that both the I(^{1}H) and S(^{13}C) spin systems tend to achieve a common spin temperature with an intrinsic time constant T_{IS} during each contact time τ_{CP} (*10–12*). Namely, the magnetizations obtained after the kth contact, $M_I^{(k)}$ and $M_S^{(k)}$, may be represented such that magnetizations after the $(k-1)$st contact may approach exponentially to the equilibrium magnetizations $M_I^{(k)eq}$ and $M_S^{(k)eq}$,

$$M_I^{(k)} = (M_I^{(k-1)} - M_I^{(k)eq})e^{-\tau_{CP}/T_{IS}} + M_I^{(k)eq},$$

$$M_S^{(k)} = (M_S^{(k-1)} - M_S^{(k)eq})e^{-\tau_{CP}/T_{IS}} + M_S^{(k)eq}, \qquad [1]$$

where the magnetizations are represented using the instantaneous spin temperatures $T_I^{(k)}$ and $T_S^{(k)}$ as

$$M_I^{(k)} = \frac{N_I \gamma_I^2 \hbar^2 B_{1I}}{4k_B T_I^{(k)}}, \quad M_S^{(k)} = \frac{N_S \gamma_S^2 \hbar^2 B_{1S}}{4k_B T_S^{(k)}}. \qquad [2]$$

Note that the above phenomenological and thermodynamical

treatment, or the spin temperature hypothesis, is appropriate on the condition of the long time-scale such that the change of the system can be regarded as quasi-static.

The forms of the equilibrium magnetizations in Eq. [1] may be derived using the energy conservation before and after the kth contact; by noting the phase inversion of the S spin system,

$$E_I^{(k)eq} + E_S^{(k)eq} = E_I^{(k-1)} - E_S^{(k-1)}, \qquad [3]$$

where

$$E_I^{(k-1)} = -\frac{N_I \gamma_I^2 \hbar^2 B_{1I}^2}{4 k_B T_I^{(k-1)}}, \quad E_S^{(k-1)} = -\frac{N_S \gamma_S^2 \hbar^2 B_{1S}^2}{4 k_B T_S^{(k-1)}},$$

$$E_I^{(k)eq} = -\frac{N_I \gamma_I^2 \hbar^2 B_{1I}^2}{4 k_B T^{(k)eq}}, \quad E_S^{(k)eq} = -\frac{N_S \gamma_S^2 \hbar^2 B_{1S}^2}{4 k_B T^{(k)eq}}. \qquad [4]$$

By assuming the exact Hartman–Hahn condition $\gamma_I B_{1I} = \gamma_S B_{1S}$, the common spin temperature for both the systems to achieve is simply given by

$$\frac{1}{T^{(k)eq}} = \frac{1}{1 + \epsilon} \frac{1}{T_I^{(k-1)}} - \frac{\epsilon}{1 + \epsilon} \frac{1}{T_S^{(k-1)}}, \qquad [5]$$

where ϵ is the ratio of the heat capacities, or the number of spins, of the individual spin systems, N_S/N_I, which is typically the order of 0.01. The equilibrium magnetizations, which would be achieved in a sufficiently long contact time, are thus formulated using the equilibrium temperature $T^{(k)eq}$ as

$$M_I^{(k)eq} = \frac{N_I \gamma_I^2 \hbar^2 B_{1I}}{4 k_B T^{(k)eq}} = \frac{1}{1 + \epsilon} M_I^{(k-1)} - \frac{1}{1 + \epsilon} \frac{\gamma_I}{\gamma_S} M_S^{(k-1)},$$

$$M_S^{(k)eq} = \frac{N_S \gamma_S^2 \hbar^2 B_{1S}}{4 k_B T^{(k)eq}} = \frac{\epsilon}{1 + \epsilon} \frac{\gamma_S}{\gamma_I} M_I^{(k-1)} - \frac{\epsilon}{1 + \epsilon} M_S^{(k-1)}. \qquad [6]$$

By substituting Eq. [6] into Eq. [1], we may obtain the relationship between the magnetizations before and after the kth *insufficient* contact time:

$$M_I^{(k)} = \frac{1 + \epsilon e^{-\tau_{CP}/T_{IS}}}{1 + \epsilon} M_I^{(k-1)} - \frac{\gamma_I}{\gamma_S} \frac{1 - e^{-\tau_{CP}/T_{IS}}}{1 + \epsilon} M_S^{(k-1)},$$

$$M_S^{(k)} = \frac{\gamma_S}{\gamma_I} \frac{\epsilon(1 - e^{-\tau_{CP}/T_{IS}})}{1 + \epsilon} M_I^{(k-1)}$$
$$- \frac{\epsilon - (1 + 2\epsilon)e^{-\tau_{CP}/T_{IS}}}{1 + \epsilon} M_S^{(k-1)}. \qquad [7]$$

These equations are regarded as simultaneous recurrence formulae, and so they can be solved with an appropriate initial condition that, here as usual, only the ^{1}H transverse magnetization exists at first:

$$M_I^{(0)} = \frac{N_I \gamma_I^2 \hbar^2 B_0}{4 k_B T}, \quad M_S^{(0)} = 0. \qquad [8]$$

After some algebra, we obtain the normalized decay function for the $I(^1$H$)$ magnetization after the Nth phase-alternating contact as

$$f(N, \tau_{CP}) \equiv \frac{M_I^{(N)}}{M_I^{(0)}} = \frac{1}{1 - \epsilon}$$
$$\times \left[\left(\frac{1 - \epsilon + 2\epsilon e^{-\tau_{CP}/T_{IS}}}{1 + \epsilon} \right)^N - \epsilon e^{-N\tau_{CP}/T_{IS}} \right]. \qquad [9]$$

It is worth examining, by following Eq. [9], how efficiently the $I(^1$H$)$ magnetization may decay. First, we consider the case that $\tau_{CP} \gg T_{IS}$, which corresponds to the situation that, during every CP contact period τ_{CP}, the equilibrium is achieved because of the comparatively short T_{IS} or long τ_{CP}. In this limit, the normalized decay function given in Eq. [9] becomes, during $\tau_{tot} = N\tau_{CP}$,

$$\lim_{\tau_{CP}/T_{IS} \to \infty} f(N, \tau_{CP}) = \frac{1}{1 - \epsilon} \left(\frac{1 - \epsilon}{1 + \epsilon} \right)^N \simeq e^{-(2N-1)\epsilon}, \qquad [10]$$

where we use $\epsilon \ll 1$. This result contrasts well to that of the original MC CP sequence where the phase of the irradiated field is not alternated and the enhanced $S(^{13}$C$)$ transverse magnetization is forced to decay during the intervals τ_{dec} between the individual contact times (*10–12*). It is known that the sequence yields the normalized decay function during $\tau_{tot} = N(\tau_{CP} + \tau_{dec})$ after the N contact times,

$$\lim_{\tau_{CP}/T_{IS} \to \infty} f(N, \tau_{CP}) = \left(\frac{1}{1 + \epsilon} \right)^N \simeq e^{-N\epsilon}, \qquad [11]$$

where the condition $\tau_{CP} \gg T_{IS}$ used here exhibits the most efficient decay in the MC CP sequence. It is obvious, by comparing Eqs. [10] and [11], that the PAMC CP may efficiently decay the $I(^1$H$)$ magnetization more than twice during a fixed total irradiation time τ_{tot}; if we assume $\tau_{dec} = \tau_{CP}$ in the MC CP sequence, during the same period of total contact time $\tau_{tot} = 2N\tau_{CP}$ the PAMC CP sequence suppresses the magnetization about four times efficiently.

It is important to find the experimental conditions which lead to the most efficient magnetization decay in the PAMC CP sequence. The experimental parameters adjustable in the sequence are the number of the contacts N and the length of each contact time τ_{CP}. As a matter of course and also as inferred from Eq. [10], the more increases the number of contacts N, the more the magnetization may be destroyed. However, an excessively long irradiation period $\tau_{tot} = N\tau_{CP}$ may cause the heating up of the sample and the RF probe circuit. We have to,
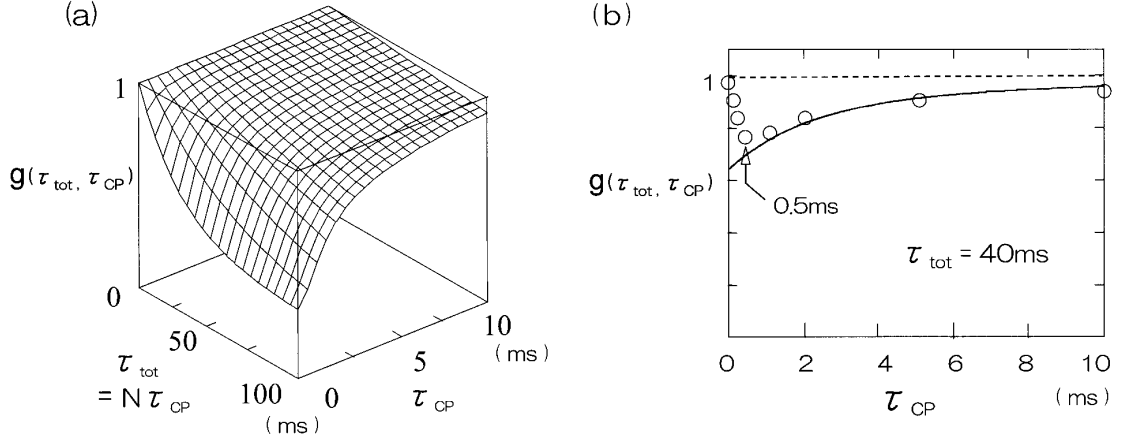
FIG. 2. Simulation of the normalized decay function $g(\tau_{tot}, \tau_{CP})$ given in Eq. [12]; for the parameters involved in the equation, $\epsilon = 0.0069$ and $T_{IS} = 1.2$ ms are assumed, which are those for adamantane. (a) The decay function of variables τ_{tot} and τ_{CP}. (b) The function of the only variable τ_{CP}, whereas τ_{tot} is fixed to be 40 ms. Open circles in (b) indicate experimental results for adamantane.

therefore, search for the efficient decay condition for a given τ_{tot} which is set to a reasonable length. For this purpose, we may as well rewrite Eq. [9] as a function of τ_{tot} and τ_{CP}:

$$g(\tau_{tot}, \tau_{CP}) = \frac{1}{1 - \epsilon} \left[\left(\frac{1 - \epsilon + 2\epsilon e^{-\tau_{CP}/T_{IS}}}{1 + \epsilon} \right)^{\tau_{tot}/\tau_{CP}} - \epsilon e^{-\tau_{tot}/T_{IS}} \right].$$

[12]

Figure 2a illustrates the behavior of the function $g(\tau_{tot}, \tau_{CP})$. As mentioned above, the longer the total contact time τ_{tot} becomes, the more the magnetization is destroyed; regardless of a given value of τ_{CP}, the function $g(\tau_{tot}, \tau_{CP})$ monotonically decreases with τ_{tot}.

A much more remarkable feature shown in Fig. 2a is that, for a given value of τ_{tot}, the more efficiently the magnetization decays as each contact time τ_{CP} decreases. In principle, in the limit of $\tau_{CP} \to 0$ and $N \to \infty$ for a fixed value of τ_{tot}, we can expect the most efficient magnetization decay as

$$g(\tau_{tot}, 0) = \frac{1}{1 - \epsilon} \left[e^{-2\epsilon\tau_{tot}/(1+\epsilon)T_{IS}} - \epsilon e^{-\tau_{tot}/T_{IS}} \right]. \quad [13]$$

Namely, we found that the $I(^1\mathrm{H})$ magnetization may be destroyed more efficiently using short τ_{CP} times with many contacts N rather than using sufficiently long $\tau_{CP} \gg T_{IS}$ discussed above; since even the latter condition was shown to be more efficient than the original phase-*un*alternating MC CP sequence, the former condition much more efficiently destroys the I magnetization. The efficacy of such a short τ_{CP} can intuitively be understood from the fact that the exponential decay as given in Eq. [1] yields the faster magnetization transfer at the initial stage rather than after a long-time contact.

In reality, however, an extremely short τ_{CP} period may violate the spin temperature hypothesis, which we used to describe the behavior of the magnetizations as in Eq. [1]. The length of the *adequately* short τ_{CP} may be determined experimentally: Fig. 2b demonstrates the comparison between the theoretical and experimental behavior of $g(\tau_{tot}, \tau_{CP})$ as a function of τ_{CP}, while τ_{tot} is fixed. The experimental results clearly show a minimum of the surviving magnetization around $\tau_{CP} = 0.5$ ms whereas it is theoretically expected to decrease monotonically with the decrease of τ_{CP}. In other words, the spin temperature hypothesis giving the theoretical curve in Fig. 2b is broken in the region shorter than $\tau_{CP} \simeq 0.5$ ms. Thus, we experimentally found the condition for the most efficient destruction of the $I(^1\mathrm{H})$ magnetization in the PAMC CP sequence, which offers the optimum magnetization to the subsequent imaging sequence as illustrated in Fig. 1. The reason why the spin temperature hypothesis is broken on the above time condition and the derivation, from the first principles, of the conditions with which the internal spin interactions of the sample are related *(12, 18)* may be of theoretical interest but out of scope in the present imaging study. The authors expect theoreticians to elucidate our observations.

Equation [9] or equivocally Eq. [12] demonstrates how the normalized decay function, $f(N, \tau_{CP})$ or $g(\tau_{tot}, \tau_{CP})$, depends on the internal but phenomenological spin parameter T_{IS}, which is an index of the magnitude of the $I(^1\mathrm{H})$–$S(^{13}\mathrm{C})$ dipolar interactions, varying from one compound to another. Therefore, those equations may predict how fast the $I(^1\mathrm{H})$ magnetization decays during the PAMC CP sequence, and how much amount of the magnetization survives after the sequence, for the samples having various values of T_{IS}. Figure 3 shows the predicted decay function $g(\tau_{tot}, \tau_{CP})$ for three different values of T_{IS}; the length of each contact time τ_{CP} is fixed to be 0.5 ms. As seen from Fig. 3, the magnitudes of the magnetizations surviving after the PAMC CP sequence of the length τ_{tot}, for example, 100 ms, can clearly be distinguished: The shorter are the cross-relaxation times T_{IS}, the more remarkably the mag-
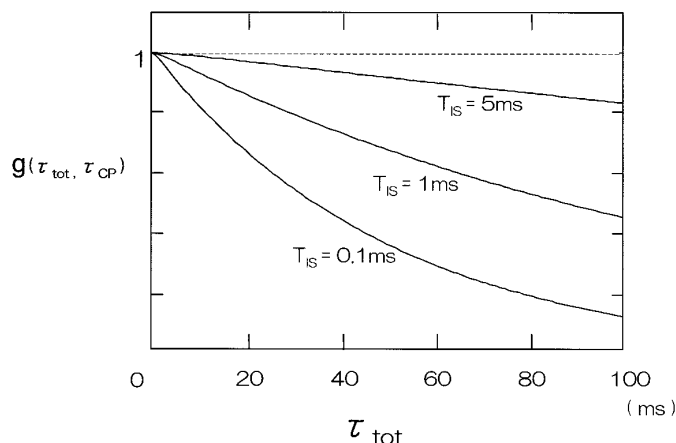
FIG. 3. Simulation of the normalized decay function $g(\tau_{tot}, \tau_{CP})$ given in Eq. [12] for three different values of $T_{IS} = 0.1$, 1, and 5 ms; the value of τ_{CP} is fixed to be 0.5 ms, while $\epsilon = 0.0069$ is assumed.

netizations may be destroyed. It is this difference of the remaining magnetizations that yields the clear contrast in observed images. Thus, we proved that the PAMC CP sequence can give rise to the T_{IS}-weighted images for solid samples, similarly to well-known T_1- or T_2-weighted images for liquid samples.

It should be noted that the discrepancy may occur between the theoretically predicted and experimentally observed decay if we use a short τ_{CP} period in the region where the spin temperature hypothesis is broken; in Fig. 2b, even the *optimal* condition of $\tau_{CP} = 0.5$ ms yields the surviving magnetization deviated from the predicted one. Such deviation may lead to artificial evaluation for the magnetization: Since the magnetization may be less destroyed in such a time region than predicted, the effective T_{IS} may apparently become larger than the genuine value as understood from Fig. 3. However, in order to destroy the magnetization the most efficiently by using $\tau_{CP} = 0.5$ ms, for example, one has to tolerate such nonideality.

Finally in this section, we mention another possible discrepancy between the theory and experiments, in addition to that originating from the short τ_{CP} behavior discussed above. Namely, it is the deviation of the practical or effective value of $\epsilon = N_S/N_I$ from the value which is *a priori* determined from the composition of the compound together with the natural abundance of the $I(^1H)$ and $S(^{13}C)$ nuclei. If the entire I and S nuclei participate in the CP process, there appears no such deviation. In practice, however, if a part of $I(^1H)$ spins only around $S(^{13}C)$ spins release their polarization, the effective value of ϵ becomes larger than the ideal value. As a result, the magnetizations of such I spins are transferred to S spins more efficiently, whereas the polarizations due to the rest of the I spins are left unchanged. Although it is difficult to describe the net effect comprised of the two reciprocal factors in such a case, we believe that we did not suffer from such an effect in the course of the experiments as shown below; since polariza-

tion transfer between protons is generally faster than that between protons and carbons, no proton is isolated.

^1H Images Obtained via PAMC CP Sequence

Figure 4 illustrates one-dimensional ^1H projection images of the phantom observed using the pulse scheme given in Fig. 1; the spatial axis indicates the direction along the MAS rotor axis, and the spectral intensities show the ^1H densities at the individual positions of the phantom. For both the spectra in Figs. 4a and 4b, a common value of the spin-locking time $\tau_{SL} = 41$ ms was adopted, whereas the number of the contacts was varied as $N = 0$ for Fig. 4a and $N = 80$ for Fig. 4b, with each contact time $\tau_{CP} = 0.5$ ms; the total contact time τ_{tot} was hence 0 and 40 ms for Figs. 4a and 4b, respectively. As mentioned in the previous section, the influence of the $T_{1\rho}$ effect during τ_{tot} was thus excluded in comparing these spectra.

In Fig. 4a are shown almost the same intensities for the parts of ferrocene (left in the figure) and diluted adamantane (right). On the other hand, however, the signals are differentiated in Fig. 4b for these two parts; about 60% of the signal intensity was reduced for the part of ferrocene, while about 20% for adamantane. This difference is attributable to the variation of the T_{IS} values for the compounds. Thus, the spectrum showing different intensities for the compounds in Fig. 4b may be regarded as a T_{IS}-weighted $I(^1H)$ image, and such images are proved to be useful for the discrimination of solid materials.

The values of T_{IS} at the individual positions, or the pixels, of the phantom can be determined by comparing Figs. 4a and 4b. The behavior of the ^1H signal decay can be simulated by the phenomenological theory described in the previous section, for example, by applying Eq. [9] or [12] to each pixel of the spectra. Figure 5a demonstrates such simulation for the representative two pixels corresponding to the parts of adamantane and ferrocene indicated by Fig. 5b. In order to determine the T_{IS} values by simulating the experimental signal intensities, only two points for the different N or τ_{tot} values are required, for example, $\tau_{tot} = 0$ and 40 ms (filled marks in Figs. 5a and 5b). In fact, the simulated curves shown in Fig. 5 are obtained in such a way; for the sake of reference, the other three points observed for $\tau_{tot} = 10$, 20, and 30 ms are depicted in Fig. 5 as open marks. The determined T_{IS} values for the chosen two pixels are 1.68 ms for the part of adamantane and 0.84 ms for ferrocene.

If the aforementioned procedure is applied to all the pixels where the sample is loaded, it follows that we may obtain a T_{IS}-mapping $I(^1H)$ image, instead of the T_{IS}-weighted $I(^1H)$ image depicted in Fig. 4b. Figure 6 shows the T_{IS} mapping for the same phantom sample. Clearly, at the positions where the compounds are, significant mapping of T_{IS} values is shown; for clarity, the positions where the compounds are loaded are shown by the spectra drawn with dashed curves. For the part of ferrocene (left in the figure), almost the common values of $T_{IS} \simeq 0.8$ ms are obtained, whereas for adamantane (right) ap-
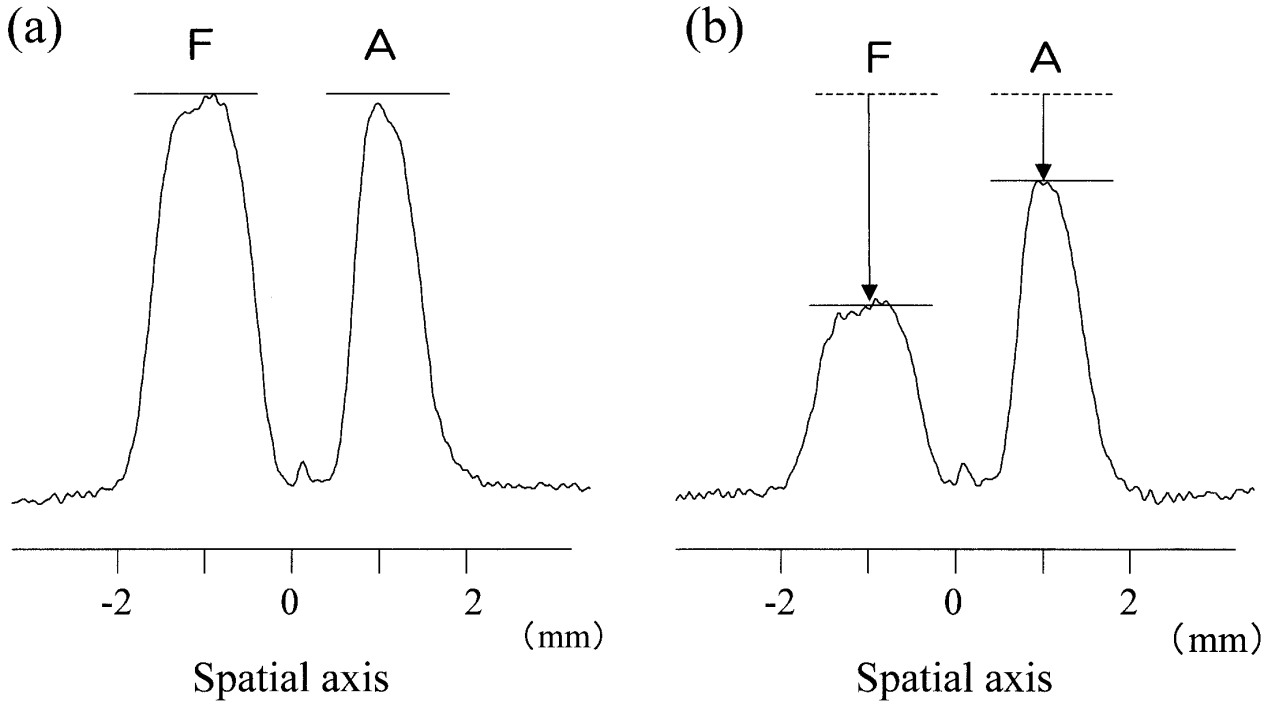
FIG. 4. One-dimensional ^1H image for a phantom constituted of ferrocene (left in the figure indicated by F) and adamantane (right indicated by A), which was observed using the experimental scheme shown in Fig. 1; experimental parameters used are $\tau_{SL} = 41$ ms, $\tau_{CP} = 0.5$ ms, and (a) $\tau_{tot} = 0$ and (b) 40 ms, respectively.

proximately 1.6 ms of T_{IS} is distributed in space. Therefore, we demonstrated that solid materials can be distinguished not only by a T_{IS}-weighted $I(^1H)$ image but also a T_{IS}-mapping $I(^1H)$

image, by using the experimental scheme in Fig. 1, or the PAMC CP ^1H imaging.

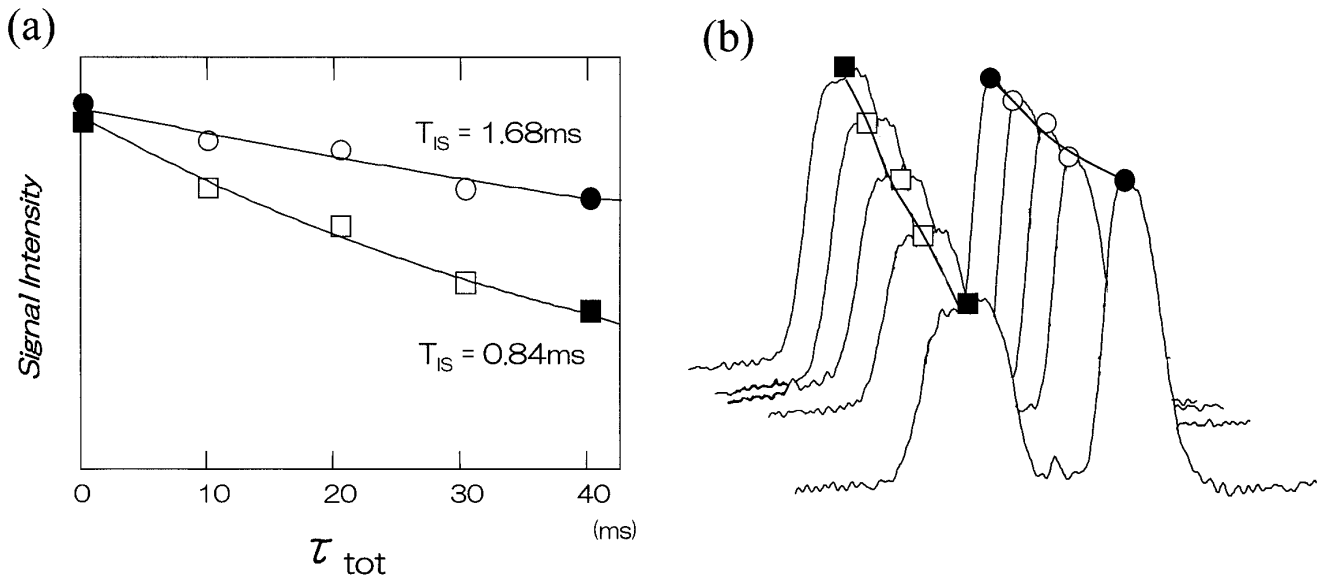The T_{IS} values themselves are determined by independent

FIG. 5. (a) PAMC CP decay function observed for the representative positions of the phantom and the corresponding simulation. The positions in the image spectrum were indicated in (b); squares for the part of ferrocene and circles for adamantane show the positions chosen as the representative ones. For simulation in (a), two time points $\tau_{tot} = 0$ and 40 ms, indicated by filled marks are used, whereas open marks are plotted for reference. Simulation was performed using the theory developed in the present paper, especially using Eq. [12].
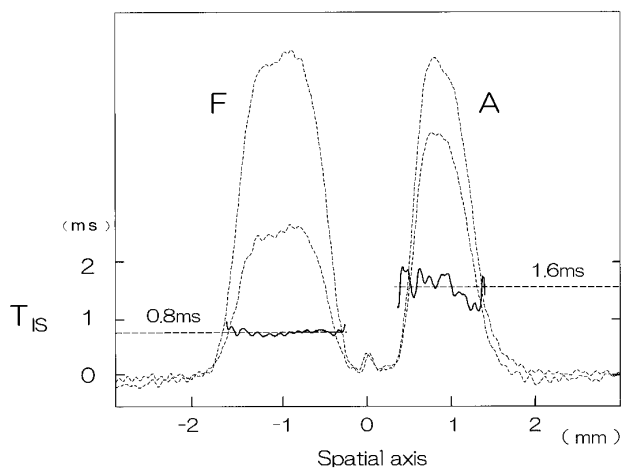
FIG. 6. T_{IS} mapping for the phantom constituted of ferrocene (left in the figure indicated by F) and adamantane (right indicated by A). T_{IS} values at the individual positions of the phantom were determined by the procedure shown in Fig. 5. For clarity, the ^{1}H images of the phantom were shown by dashed curves.

and conventional spectroscopy (*12*) for the individual compounds. Thereby, $T_{IS} \simeq 1.2$ and 0.7 ms for adamantane and ferrocene were respectively evaluated. For both the compounds, the PAMC CP T_{IS} mapping shows rather longer T_{IS} values than those from the spectroscopy. This apparent disagreement may call the readers' attention or even doubt against the quantitativeness of the method. Such deviation may be caused by the short-time behavior of the magnetization during each contact period τ_{CP}, as discussed in the previous section; seemingly larger surviving ^{1}H magnetizations mislead larger values of T_{IS} as understood from Fig. 3. As shown in Fig. 2b, the experimental condition of $\tau_{CP} = 0.5$ ms exhibits slight departure from the theoretical curve predicted by the spin temperature hypothesis, even though the condition is *optimal* in the sense that most efficiently the ^{1}H magnetization is to be destroyed. Thus, we recommend the following strategies in the PAMC CP ^{1}H imaging: When one requires only the discrimination of compounds by their relative T_{IS} values, he or she should use the above *optimal* condition to clarify the difference more, as we did in the present study; when one needs more exact T_{IS} values distributed in space, he or she should appeal to use longer τ_{CP} values at the cost of some degradation for the discrimination. In either case, the PAMC CP may yield a solution.

CONCLUSION

In the present paper, we have shown a novel method for observing ^{1}H images reflecting ^{1}H–^{13}C dipolar interactions, via cross relaxation time T_{IS}, for solid-state materials. Phase-alternating multiple-contact cross polarization (PAMC CP) was used to prepare the ^{1}H magnetization which decays partly but efficiently, while the TREV-8 sequence with field gradients

was incorporated for solid-state ^{1}H imaging. The efficiency of the PAMC CP sequence was evaluated using a phenomenological theory which assumes spin temperature hypothesis; analytical expression was derived for the ^{1}H magnetization after *N*-time phase-alternating contacts. It was demonstrated, by simulation and experiments, how the initial ^{1}H magnetization might be destroyed depending on the magnitudes of T_{IS}, although at the same time the limitation of the theory attributable to the spin temperature hypothesis was pointed out.

The T_{IS}-weighted contrast ^{1}H image was obtained by using the PAMC CP imaging scheme for a phantom constituted of adamantane and ferrocene; these compounds were clearly distinguished by the difference of their T_{IS} values in spite of the same order of T_{IS}'s. The scheme therefore promises much clearer contrast for mobile and rigid materials which may possess the different orders of T_{IS} values. Also, the T_{IS} mapping for the same phantom was obtained from the comparison between the experimental T_{IS}-weighted ^{1}H images and the corresponding simulation. The resultant mapping properly indicated that the two compounds have the approximately twice different T_{IS} values, which was enough for discriminating the compounds although the quantitativeness for T_{IS} values may be degraded by the limitation of the theory mentioned above. It was suggested that the choice of the experimental parameters, each contact time τ_{CP} above all, be important for evaluating the spatial distribution of T_{IS} values more quantitatively.

The PAMC CP sequence utilized in the present imaging study may be contrived probably by many other NMR spectroscopists. Since the sequence suppresses both the $I(^1$H) and $S(^{13}$C) signals, its utility for spectroscopy is limited. On the other hand, however, in NMR imaging the suppressed signals may provide useful spatial information as less intense pixels or voids. In this sense, the PAMC CP sequence finds out its significant applications in NMR imaging.

EXPERIMENTAL

The NMR experiments were performed on a Chemagnetics CMX300 Infinity spectrometer with operating resonance frequencies of 300.52 MHz for ^{1}H and 75.57 MHz for ^{13}C. A solid-state imaging probe with standard CPMAS (magic-angle spinning) capability was assembled by JEOL. All the experiments were, however, performed for stationary samples. The RF-field strength of 75 kHz for ^{1}H was applied for CP (*9–12*) and magic-echo sequence TREV-8 (*14, 15*). The time unit of the TREV-8 sequence τ was 7 μs so that the cycle time of the sequence $t_c = 12\tau$ was 84 μs. During the CP contact, the ^{13}C RF field satisfying the Hartmann–Hahn matching condition (*9*) was applied.

The field gradients for ^{1}H imaging were provided by Techron 7570 power supply amplifiers, with a gradient controller from JEOL. A gradient parallel to the external high magnetic field, G_z, and another gradient perpendicular to it,

G_y, were used to produce a gradient along the MAS rotor axis, $G = 18.5$ mT/m. The gradient was switched in about 25 μs.

The samples of adamantane $C_{10}H_{16}$ and ferrocene $C_{10}H_{10}Fe$ were chosen as the compounds which have different magnitudes of internal ^{13}C–^1H dipolar interactions due to the difference of the molecular motions (*16*). KBr (potassium bromide) and PTFE (polytetrafluorethylene) were used as spacers for making an "imaging phantom"; the former is also used to dilute adamantane. The phantom is made by using a PTFE spacer specially designed to have a ring vacancy in an MAS rotor (*17*) for better magic-echo line narrowing. The molded ring samples are loaded in the MAS rotor having the PTFE spacer, with their centers concentric: The phantom is constituted of a 1-mm-thick ferrocene ring and a 0.6-mm-thick diluted adamantane ring, both of which are separated by a 1-mm-thick KBr ring.

Theoretical simulation was performed on a PC/AT compatible computer, where Free BSD unix was installed. Calculations were made from a program written in FORTRAN-77 and compiled with a GNU compiler.

ACKNOWLEDGMENTS

REFERENCES

1. D. G. Cory, *Annu. Rep. NMR Spectrosc.* **24,** 87–180 (1992); P. Blümler and B. Blümich, *in* "NMR—Basic Principles and Progress," Vol. 30, pp. 209–277, Springer-Verlag, Berlin (1993).

2. S. Matsui, *Chem. Phys. Lett.* **179,** 187–190 (1991).

3. D. E. Demco, S. Hafner, and R. Kimmich, *J. Magn. Reson.* **96,** 307–322 (1992).

4. F. Weigand, B. Blümich, and H. W. Spiess, *Solid State NMR* **3,** 59–66 (1994).

5. P. Mansfield and P. Morris, "NMR Imaging in Biomedicine," Academic Press, New York (1982).

6. P. T. Callaghan, "Principles of Nuclear Magnetic Resonance Microscopy," Clarendon, Oxford (1991).

7. F. Weigand, D. E. Demco, B. Blümich, and H. W. Spiess, *Solid State NMR* **6,** 357–365 (1996).

8. S. Matsui, M. Nonaka, T. Nakai, and T. Inouye, *Solid State NMR* **10,** 39–44 (1997).

9. S. R. Hartmann and E. L. Hahn, *Phys. Rev.* **128,** 2042–2053 (1962).

10. A. Pines, M. G. Gibby, and J. S. Waugh, *J. Chem. Phys.* **59,** 569–590 (1973).

11. P. K. Grannell, P. Mansfield, and M. A. B. Whitaker, *Phys. Rev. B* **8,** 4149–4163 (1973).

12. M. Mehring, "High Resolution NMR in Solids," 2nd ed., Chap. 4, Springer-Verlag, Berlin (1983).

13. W. Kuhn, P. Barth, S. Hafner, G. Simon, and H. Schneider, *Macromol.* **27,** 5773–5779 (1994); C. Fülber, D. E. Demco, and B. Blümich, *Solid State NMR* **6,** 213–223 (1996).

14. W-K. Rhim, A. Pines, and J. S. Waug, *Phys. Rev. B* **3,** 684–695 (1971).

15. K. Takegoshi and C. A. McDowell, *Chem. Phys. Lett.* **116,** 100–104 (1985).

16. C. A. Fyfe, "Solid State NMR for Chemists," C. F. C. Press, Guelph (1983).

17. N. Ch. Nielsen, H. Bildsøe, and H. J. Jakobsen, *J. Magn. Reson.* **98,** 665–673 (1992).

18. D. Demco, J. Tegenfeldt, and J. S. Waugh, *Phys. Rev. B* **11,** 4133–4151 (1975).